Computational Insights into the Electronic, Optical, and Reactivity Behavior of Halogenated Phenanthrene Derivatives

Rebaz A. Omer[1,2], Khdir A. Othman[1], Yousif H. Azeez[3], and Aryan F. Qader[1†]

[1]Department of Chemistry, Faculty of Science and Health, Koya University, Danielle Mitterrand Boulevard,
Koya KOY45, Kurdistan Region – F.R. Iraq

[2]Department of Pharmacy, College of Pharmacy, Knowledge University,
Erbil, 44001, Kurdistan Region – F.R. Iraq

[3]Department of Physics, University of Halabja, College of Science,
Halabja, Kurdistan Region – F.R. Iraq

Abstract—**This study explores the complex effects of halogenation on polycyclic aromatic hydrocarbons (PAHs), specifically focusing on phenanthrene. The research aims to understand how the substitution of halogens – namely fluorine (F), chlorine (Cl), and bromine (Br) – in the phenanthrene structure affects its electronic properties, reactivity, and potential applications. The results indicate that halogenation reduces the HOMO-LUMO gap by 0.0100 eV, 0.0064 eV, and 0.2438 eV for F, Cl, and Br, respectively. In addition, it increases the electronegativity (e.g., phenanthrene: 3.6371 eV; phenanthrene-Br: 3.8575 eV), enhancing electron attraction from the phenanthrene rings and lowering the chemical potential. Through detailed analyses of molecular orbitals and density of states, the study reveals significant shifts in energy levels and optical properties. It also employs NMR spectroscopy, potential energy maps, and charge distribution to provide a comprehensive understanding of the compounds. Reduced Density Gradient and Non-Covalent Interaction (NCI) analyses further elucidate the complexities of intermolecular forces in the halogenated derivatives. The research delves into drug-likeness, Natural Bond Orbital (NBO) analysis, and Non-linear Optical properties, highlighting potential applications in medicine, environmental science, and organic electronics. Notably, the halogenated molecules exhibit more intense coloration compared to undoped phenanthrene, with absorption peaks shifting to $\lambda = 295.1$ nm for phenanthrene-Cl, 305.3 nm for phenanthrene-F, and 307.2 nm for phenanthrene-Br, compared to $\lambda = 293.0$ nm for pure phenanthrene. These findings underscore the transformative impact of halogenation, positioning this study as a significant contribution to the understanding and potential utilization of halogenated PAHs.**

Index Terms—**Density functional theory, Doping, Electronic behavior, Energy gap, Halogen, Polycyclic aromatic hydrocarbons chemistry.**

I. Introduction

Polycyclic aromatic hydrocarbons (PAHs) are organic compounds characterized by multiple aromatic rings fused in unique and intricate arrangements. Among these, phenanthrene stands out, alongside other well-known PAHs such as naphthalene and anthracene, contributing significantly to the rich chemistry of this class of compounds (Roy, Karmakar and Dash, 2024, Omer, et al., 2024). These molecules exhibit distinct structural features and possess a wide range of versatile chemical and physical properties, making them valuable in various scientific and industrial applications. In recent years, considerable attention has been directed toward the process of halogenation, where the incorporation of halogen atoms such as fluorine, chlorine, or bromine into the PAH structure introduces new dimensions to their functionality. This modification not only alters the electronic and steric characteristics of PAHs but also enhances their potential for use in fields such as materials science, pharmaceuticals, and environmental studies (Tang, et al., 2018, Li, et al., 2024). Halogenation precisely modifies PAHs, altering their electronic structures and reactivity. The intentional introduction of halogens leads to changes in energy levels, absorption spectra, and fluorescence behaviors (Lawal and Fantke, 2017, Omer, Koparir and Ahmed, 2022b). This transformation influences the charge distribution within the phenanthrene framework, leading to noticeable yet nuanced electronic rearrangements. These subtle shifts in electron density highlight the redistribution of charges across specific molecular orbitals (MOs), altering the electronic environment of the system. Such modifications can significantly impact the molecule's overall reactivity, stability, and potential interactions, offering valuable insights into its chemical behavior under varying conditions (Ding, Tommasini and Maestri, 2019, Rebaz, et al., 2022, Arcadi, et al., 2023). Laying the groundwork for understanding the reactivity of halogenated PAHs is essential. Halogenated phenanthrene derivatives provide a versatile avenue for

exploration. In medicine, these derivatives exhibit potent antibacterial and antifungal properties, indicating their potential therapeutic applications (McCoull, et al., 1999, Omar, et al., 2023). Their adaptability in cancer treatment and infection control, along with the formation of intricate metal complexes, paves the way for advanced drug delivery (Sahoo, et al., 2020, Koparir, et al., 2022). In the environment, halogenated PAHs leave distinct footprints, altering their persistence and toxicity (Barbosa, et al., 2023, Palmer, et al., 2009). Halogenation enhances the optoelectronic properties of phenanthrene, highlighting its potential applications in organic photovoltaic cells, OLEDs, and field-effect transistors (Haritash and Kaushik, 2009, Ahmed and Rebaz, 2020, Abdel-Shafy and Mansour, 2016, Li and Wu, 2023, Li, et al., 2020). Despite the comprehensive findings, several gaps in this study warrant further investigation. Although the electronic, optical, and chemical properties of halogenated phenanthrene derivatives are extensively analyzed, the effects of halogenation on their thermal stability and mechanical properties remain unexplored. Furthermore, the long-term environmental effects and degradation pathways of halogenated PAHs have yet to be studied, which is critical for understanding their ecological impact. While potential applications in organic electronics and medicine are discussed, there is a lack of experimental validation of these properties in practical devices or biological systems. The goal of the research is to gain insight into how the substitution of halogens – fluorine (F), chlorine (Cl), and bromine (Br) – within the phenanthrene structure affects its electronic properties, reactivity, and potential applications. Fluorine, chlorine, and bromine are commonly chosen for the halogenation of phenanthrene because of their unique chemical and physical properties, which influence the molecule's reactivity, electronic structure, and interactions.

II. Computational Details

In this research investigation, the method of Density Functional Theory (DFT) was harnessed to perform detailed calculations. These calculations were executed using the sophisticated Gaussian 09 computational software package, which is renowned for its capabilities in simulating and modeling molecular systems. Specifically, the B3LYP functional, a widely used functional in DFT, was chosen for molecular optimization. This involved intricately refining the arrangement of atoms within the molecules to achieve their most energetically stable configurations (Montgomery, et al., 1999, Koparir, et al., 2023, Omer, et al., 2022a). The 6-31G(d,p) basis sets represent the electron orbitals as a combination of Gaussian functions. These basis sets improve accuracy by including polarization functions (d,p) and diffuse functions (++, for anions or systems with long-range interactions). For DFT Calculations in Gaussian: Functional: B3LYP, Basis Set: 6-31G (d,p), Optimization: Opt=(tight), Frequency Analysis: Freq=NLO (to compute thermodynamic and NLO properties) and Charge and Multiplicity: Set according to the system (e.g., neutral or ionic), Fig. 1.

III. Results and Discussion

Phenanthrene and its derivatives doped with fluorine, chlorine, and bromine were meticulously designed through Gauss View. Subsequently, a DFT model was employed to optimize their structures using the suitable B3LYP/6-311G basis set known for its adeptness in capturing accurate configurations (Costa, et al., 2013; Tirado-Rives and Jorgensen, 2008; Nasidi, et al., 2022).

A. MOs and Density of States (DOS) Analysis

The frontier MOs are the Highest Occupied MO (HOMO) and the Lowest Unoccupied MO (LUMO) of a molecule. They represent the ability of a molecule to donate and accept electrons, respectively. They also determine the chemical stability and reactivity of a molecule (Aihara, 1999, Sun and Wu, 2012). The energy gap between the HOMO and the LUMO is called the HOMO-LUMO gap, and it affects the optical properties of a molecule. The smaller the gap, the lower the energy and the higher wavelength of light that can excite the electrons from the HOMO to the LUMO (Clar, 1972, Becke, 1993, Aziz, et al., 2017). Fig. 2 shows that different halogens have different effects on the HOMO-LUMO gap, with fluorine having the smallest effect and bromine having the largest effect. This is because different halogens have different electronegativities, which affect how strongly they pull the electrons toward themselves. The HOMO-LUMO gap values of all molecules are reduced by substitution. The gap values of phenanthrene decrease by 0.0100, 0.0064, and 0.2438 eV upon substitution with -F, Cl, and Br atoms, respectively. Halogenated phenanthrene's negligible bandgap reduction suggests that halogenation causes minor electronic changes without substantially altering the molecule's basic characteristics. The stability and functioning of the original molecule are preserved, but these modifications are enough to affect applications that call for the fine-tuning of electronic properties.

Fig. 3 shows a DOS analysis of phenanthrene and its halogen-doped structures. A DOS analysis is a way of calculating the number of states per unit energy range that are available for electrons to occupy in a material1 (Wilbur, et al., 1982, Toriyama, et al., 2022, Sarmah and Hobza, 2020). A DOS analysis can reveal the electronic structure, band gap, and conductivity of a material. Phenanthrene has a large band gap of about 4.7186 eV, so it is an insulator or a poor conductor of electricity. The image also shows that doping phenanthrene with halogens reduces the band gap and increases the number of states near the Fermi level, which is the highest energy level occupied by electrons at zero temperature. This means that doping phenanthrene with halogens makes it more conductive or metallic.

The quantum chemical properties of phenanthrene and its halogen-substituted derivatives (Table I) exhibit a consistent trend with increasing halogen atom size. The total energy consistently decreases (Lazarou, et al., 2001), ranging from −14684.9890 eV for phenanthrene to −84714.3302 eV for phenanthrene-Br, due to the stabilizing effect of
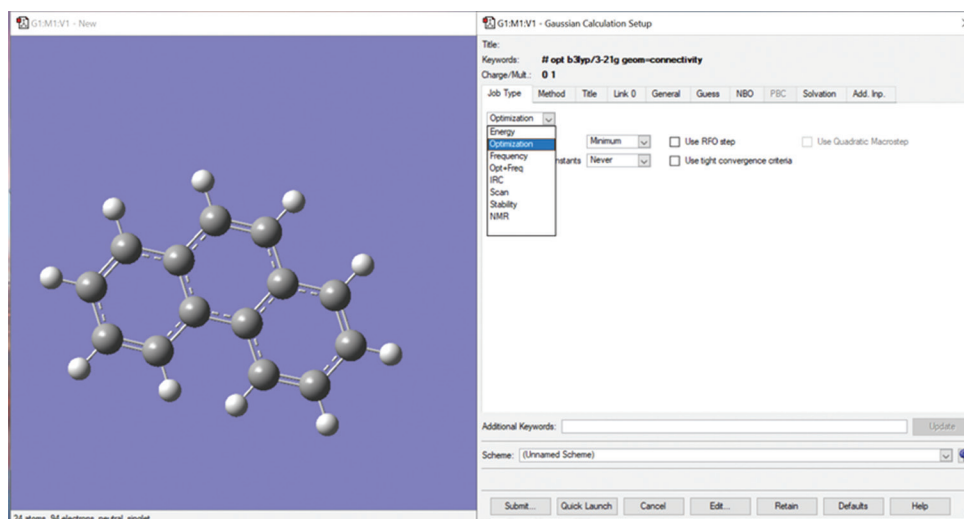
Fig. 1. The input molecule for the density functional theory calculation and the program setup.
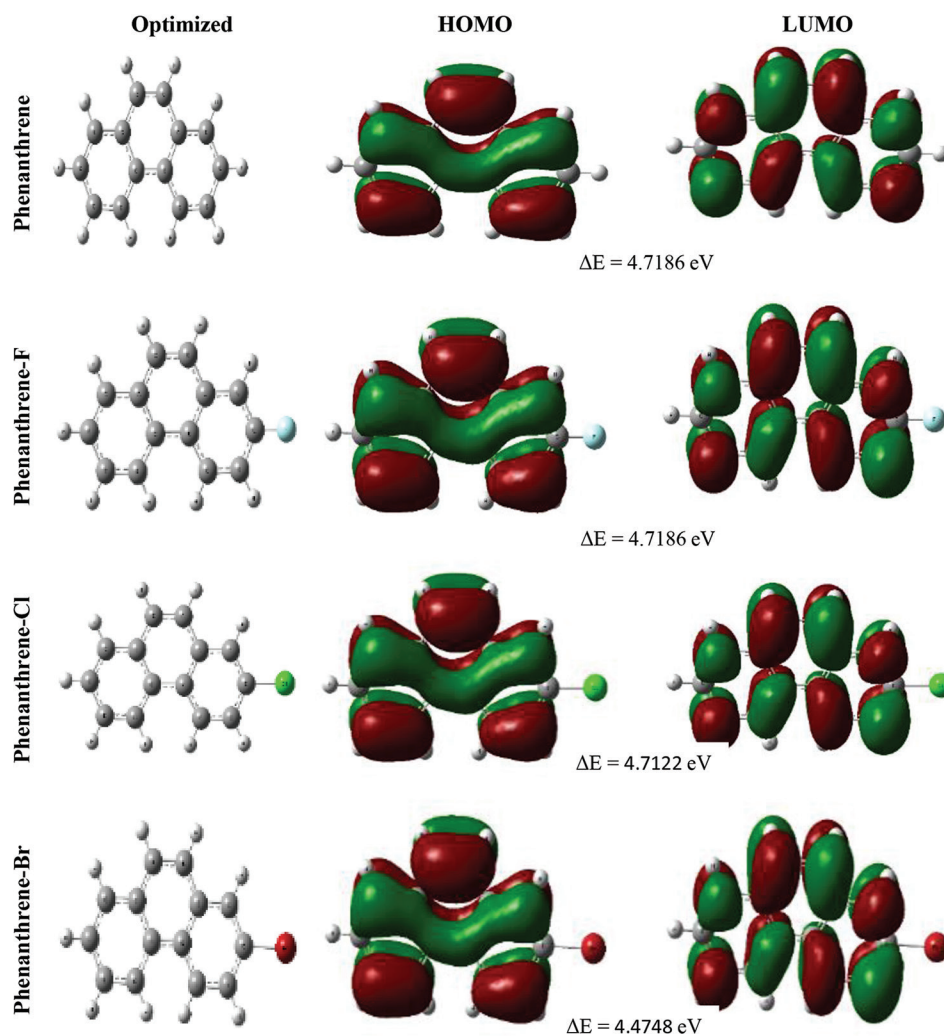

Fig. 2. Optimized structures and MOs of phenanthrene and its structures doped with halogens.

larger halogen atoms with extra electrons. Simultaneously, both HOMO and LUMO energies decrease because of the heightened electronegativity of larger halogen atoms, resulting in enhanced electron repulsion. As a result, the energy gap between HOMO and LUMO energies contracts in the sequence phenanthrene > phenanthrene-F > phenanthrene-

Cl > phenanthrene-Br, reflecting augmented polarizability and heightened reactivity within the compounds (Tang and Bao, 2011, Akbas et al., 2023, Wang, et al., 2016, Kaka, et al., 2024).

Halogen doping increases the ionization energy (I = -E_{HOMO}) and electron affinity (A = -E_{LUMO}) of phenanthrene. The IP values range from 5.9964 eV for phenanthrene to 6.0949 eV for phenanthrene-Br, making electron removal harder. The EA values range from 1.2778 eV for phenanthrene to 1.6201 eV for phenanthrene-Br, making electron addition easier (Janietz, et al., 1998).

Larger halogens lower the chemical hardness (η) and raise the softness (S) of phenanthrene and its derivatives,

because of the reduced HOMO-LUMO gap and altered polarizability and reactivity (Pearson, 2005). The η values vary from 2.3593 eV for phenanthrene to 2.2374 eV for phenanthrene-Br, while the S values vary from 0.4239 eV-1 for phenanthrene to 0.4469 eV-1 for phenanthrene-Br.

Doping phenanthrene with halogens leads to an increase in the compounds' electronegativity (phenanthrene: 3.6371 eV, phenanthrene-Br: 3.8575 eV), intensifying electron attraction from the phenanthrene rings. This results in decreased chemical potential, making the compounds more prone to electron donation to other substances.

The electrophilic nature of the halogens modulates the electrophilicity (ω) and nucleophilicity (Nu) of phenanthrene
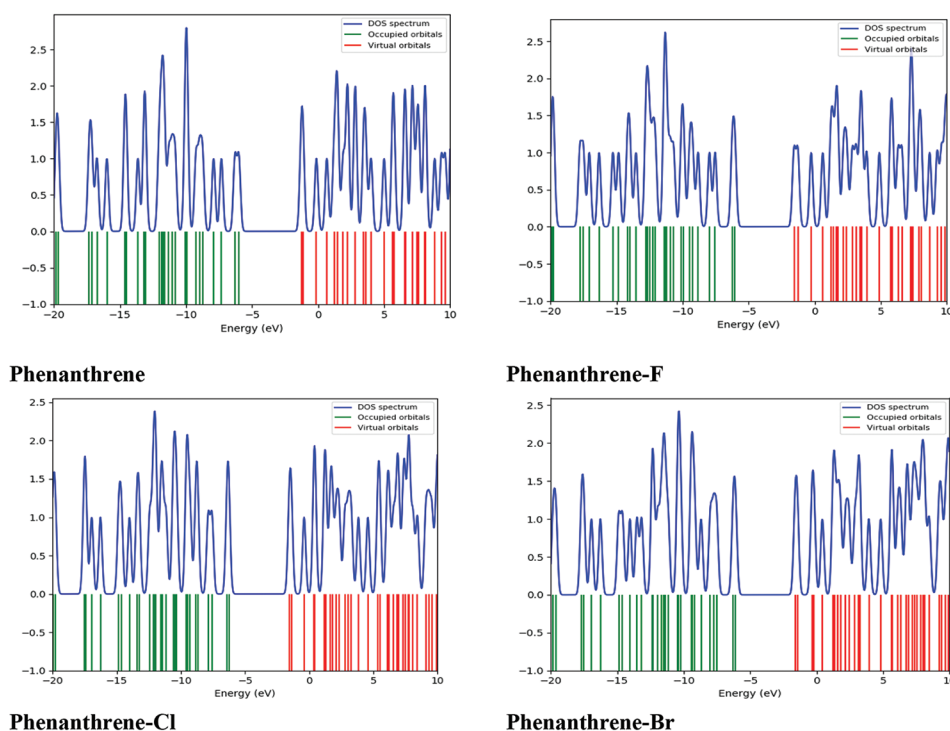

Fig. 3. DOS analysis for phenanthrene and its halogen-doped structures.

TABLE I
QUANTUM CHEMICAL PARAMETER'S VALUES OF STUDY COMPOUNDS

Quantum chemical parameters	Phenanthrene	Phenanthrene-F	Phenanthrene-Cl	Phenanthrene-Br
Total Energy (eV)	−14684.9890	−17386.1068	−27191.9416	−84714.3302
E_{HOMO} (eV)	−5.9964	−6.1925	−6.2557	−6.0949
E_{LUMO} (eV)	−1.2778	−1.4839	−1.5435	−1.6201
ΔE (eV)	4.7186	4.7086	4.7122	4.4748
Ionization potential "I" (eV)	5.9964	6.1925	6.2557	6.0949
Electron affinity "A" (eV)	1.2778	1.4839	1.5435	1.6201
Chemical hardness "η" (eV)	2.3593	2.3543	2.3561	2.2374
Chemical softness "S" (eV−1)	0.4239	0.4248	0.4244	0.4469
Electronegativity "χ" (eV)	3.6371	3.8382	3.8996	3.8575
Chemical potential "μ"(eV)	−3.6371	−3.8382	−3.8996	−3.8575
Electrophilicity "ω" (eV)	2.8035	3.1286	3.2271	3.3254
Nucleophilicity "Nu" (eV-1)	0.3567	0.3196	0.3099	0.3007
ΔE back donation	−0.5898	−0.5886	−0.5890	−0.5593
transfer electron fraction ΔN (Fe)	3.9670	3.7220	3.6524	3.5155
Dipole- moment (Debye) "μD"	0.0377	1.7148	2.3261	2.1622

and its derivatives. The ω values exhibit an ascending trend from 2.8035 eV for phenanthrene to 3.3254 eV for phenanthrene-Br, while the Nu values display a descending trend accordingly (Chattaraj and Roy, 2007, Mayr and Patz, 1994).

The back-donation energy (ΔE) is a measure of the energy difference between the HOMO of the donor and the LUMO of the acceptor. The transfer electron fraction (ΔN) is a measure of the charge transfer from the donor to the acceptor. The halogen doping affects both parameters by lowering the HOMO energy and increasing the electronegativity of phenanthrene. Phenanthrene has a higher HOMO energy and a lower electronegativity, which makes it more favorable and efficient for electron donation to iron.

B. Ultraviolet-Visible (UV-Vis) Analysis

Energy calculations used Gaussian software, optimizing the structure through the 6-311G (d,p) basis set. Employing the TD-SCF method, electronic transitions, and absorption spectrum were analyzed (Ceylan, et al., 2016; Esme, 2019; Jagdale, et al., 2020). Fig. 4 displays the absorption coefficient against incident light wavelength, revealing higher coefficients signify increased light absorption.

Phenanthrene possesses a series of conjugated double bonds, which impart them with various intriguing properties, notably their capability to absorb UV light (Li and Draine, 2002; Arfsten, et al., 1996; Wu, et al., 2010).

Doping phenanthrene with the first three halogens increases electron density in the HOMO and LUMO orbitals. This reduces the energy gap between the HOMO and LUMO orbitals and affects the optical properties of PAH molecules. The electrons at the HOMO of the doped molecules require

energy at a lower frequency and higher wavelength to transition from HOMO to LUMO (Makula, et al., 2018). This phenomenon enhances the likelihood of the doped molecules absorbing light in the visible spectrum (Fig. 4). As a result, the doped molecules exhibit more pronounced coloration compared to the undoped molecules (i.e., λ = 293.0, 295.1, 305.3, and 307.2 nm for Phenanthrene, Phenanthrene-Cl, Phenanthrene-F, and Phenanthrene-Br, respectively).

C. Infrared (IR) Analysis

Gaussian software was employed for energy calculations, yielding the optimized structure with the 6-311G (d,p) basis set (Li and Draine, 2002; Wodrich, et al., 2007).

The identification of conjugated rings within the phenanthrene structure is straightforward through aromatic C–H stretching patterns. Notably, the C−H stretching vibrations of PAHs are typically observed around 3100 cm^{-1} (Swofford, Long and Albrecht, 1976; Ricks, Douberly and Duncan, 2009; McClellan and Pimentel, 1955; Srivastava and Singh, 2007). In this study, the theoretically calculated aromatic C–H stretching vibrational modes fall within the range of 3155–3205 cm^{-1} (Fig. 5).

Exploring the repercussions of halogen doping on the IR spectra of the phenanthrene molecule reveals significant transformations. Primarily, introducing halogen atoms prompts shifts in absorption peak positions, signifying modifications in molecular vibrations and bond strengths (e.g., C=C-H in undoped phenanthrene at 3155–3205 cm^{-1}, shifting to 3292–3332 cm^{-1} for fluorine-doped phenanthrene). Novel absorption bands also emerge, showing the inception of fresh vibrational modes and functional groups. Alterations in intensity and bandwidth for
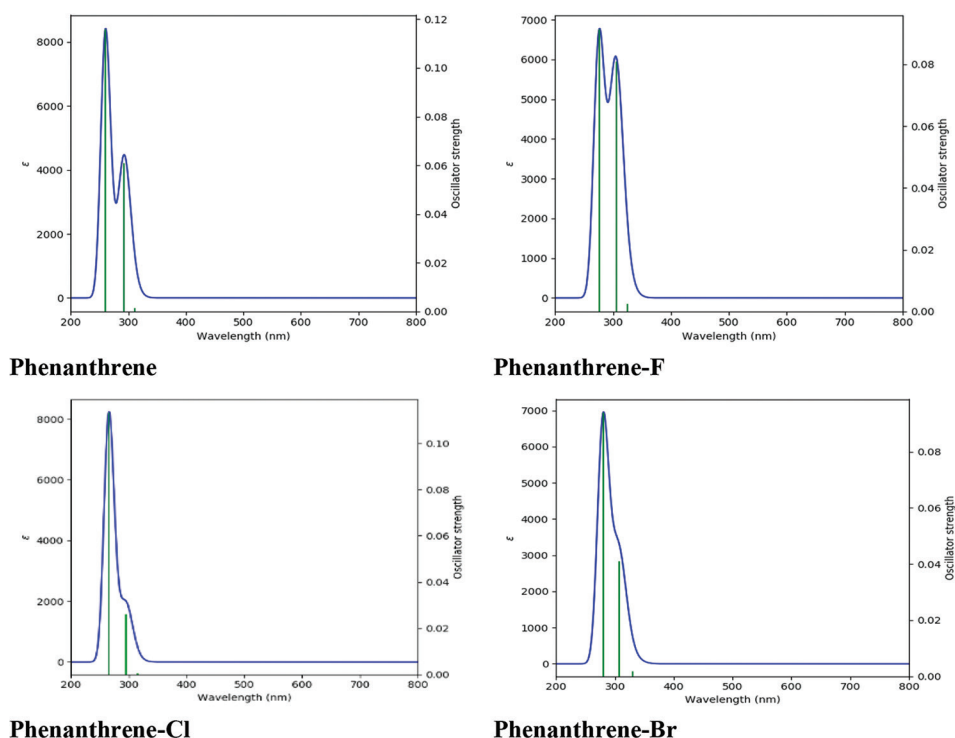
Phenanthrene

Phenanthrene-F

Phenanthrene-Cl

Phenanthrene-Br

Fig. 4. UV-Vis. absorption spectra of phenanthrene and its halogen-doped derivatives (ε is represented for absorption).

specific absorption peaks point to fluctuations in molecular flexibility and rigidity.

D. Nuclear Magnetic Resonance (NMR)

Fig. 6 shows the theoretically computed H-NMR and C-NMR structures of normal phenanthrene that doped with the first three members of the halogen group. The NMR calculations were performed using the Gaussian 09 software package. The shielding range for normal phenanthrene is from −50 to 100 ppm (Arumugam, et al., 2013). When fluorine was introduced into the compound, there was a shift in ppm from −100 to 350 ppm. The changes in ppm continued when fluorine was replaced with chlorine from −200 to 600 ppm. The changes in ppm were intense when

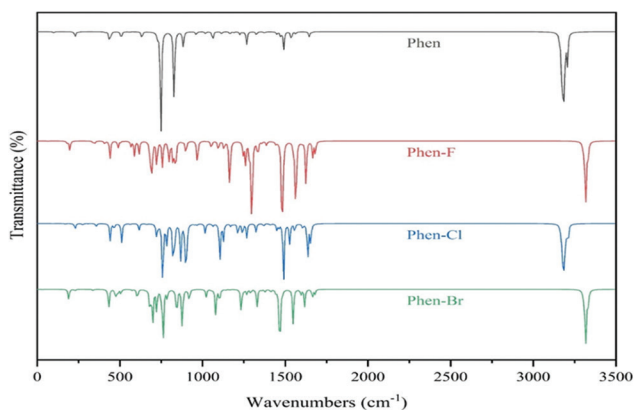bromine was introduced from −500 to 2000 ppm. This shows that the shielding range increased with an increase in the halogen's electronegativity family.

The normal NMR peaks of undoped phenanthrene show more carbon at the upfield and less carbon at the downfield. However, when fluorine was introduced, the entire orientation of the molecules changed. A sharp medium peak of fluorine appears at 289.317 ppm, and both carbon atoms and hydrogen atoms change their chemical environment because of inductive and neighboring effects. The same trend occurred when fluorine was replaced with chlorine and, later, bromine; they have peaks at 703.184 and 1975.342 ppm, respectively. This proves that NMR peaks generated by members of the halogen family in phenanthrene have a close linear relationship with their electronegativity.

E. Potential Energy Map (PES) and Charge Distribution

The PES and charge distribution are important factors that affect the molecular orientation and the optical and electrical properties of the molecules (Haenen, 1977; Solano and Mayer, 2015; Ahmed and Rebaz, 2020; Pi, et al., 2019; Ryno, 2015). Fig. 6 shows the PESs of phenanthrene and its halogen-doped derivatives. These maps illustrate how the electron density of a molecule varies in three dimensions, using different colors to show high and low charge density regions. In phenanthrene, which comprises hydrogen and carbon, the electrons are mainly localized around the rings because of the resonance effect of the double bonds, which is stronger than the electronegativity difference between carbon and hydrogen atoms. However, when fluorine is introduced as a dopant, it

Fig. 5. IR spectrum for phenanthrene and its halogenated derivative.
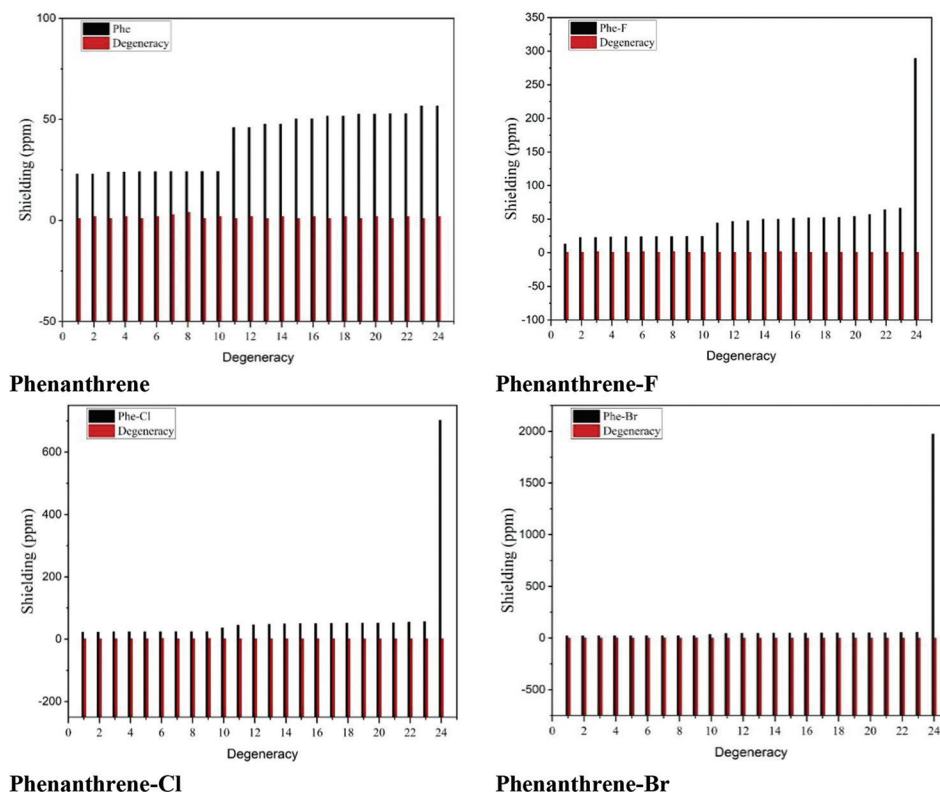

Fig. 6. NMR of phenanthrene and its halogen-doped derivatives.

alters the molecular orientation of phenanthrene. Fluorine has a higher electron affinity than carbon and hydrogen (Modelli, Mussoni and Fabbri, 2006) and thus attracts electrons toward it, resulting in a significant shift of electron density. Similar effects are observed when chlorine and bromine replace hydrogen atoms, making these atoms the most reactive sites of the doped molecule. The charge distribution in a molecule determines its physical and chemical properties. Halogen doping induces changes in charge separation and dipole moment. Halogens have higher electronegativity than carbon and thus draw more electrons, leading to an increased dipole moment and enhanced charge separation. The arrows in Fig. 7 represent the direction and magnitude of the dipole moments of each molecule. The dipole moment (μ) is a measure of molecular polarity, with larger values showing higher polarity. Fig. 7 shows that the net dipole moment follows the order of Cl > Br > F > undoped phenanthrene molecule. This trend suggests that chlorine-doped compounds exhibit the highest polarity, followed by bromine-doped compounds and then fluorine-doped ones.

F. Reduced Density Gradient (RDG) and Non-Covalent Interactions (NCI)

The utilization of RDG and NCIs in scientific inquiry has introduced innovative methodologies for comprehending and dissecting subtle intermolecular forces. The NCI index serves as a pivotal tool for delineating intermolecular interactions and scrutinizing the attributes inherent to feeble molecular affinities. Calculated through the RDG method, the NCI index furnishes empirical substantiation in favor of NCIs. The RDG, a dimensionless parameter, amalgamates density,

and its first derivative in its formulation, depicted by the following mathematical expression (Domingo, et al., 2002; Asath, et al., 2016; Boukabcha, et al., 2023).

$$RDG(r) = \frac{1|\nabla \rho(r)|}{2\left(3\pi r^2\right)^{\frac{1}{3}} \rho^{\frac{4}{3}}(r)}$$

Elaborating on this, the visually striking RDG scatter plots were generated through the utilization of the Multiwfn software (Lu and Chen, 2012), while the three-dimensional isosurfaces were visualized using the VMD software (Humphrey, Dalke and Schulten, 1996). The investigative NCI assessments were conducted employing an isosurface threshold of 0.5. It should be noted that the spectrum of the RDG isosurface ranges from −0.035 to 0.02 atomic units. The graphical representation of these molecular attributes is aptly illustrated in Fig. 8, portraying both the bi-dimensional reaction-diffusion grid (RDG) plots and their corresponding three-dimensional isosurfaces.

Significantly enhancing the characterization and quantification of molecular interactions is the graphical portrayal of the function ρ(r) with the sign of λ2. This determination of sign (λ2) bears substantial implications in predictive analyses. The negative sign of the second eigenvalue, signifying sign (λ2) ρ < 0, denotes an attractive interaction, often denominated as a bound interaction. In contrast, a positive sign of sign (λ2) ρ > 0 points to the existence of a repulsive interaction, specifically typifying a non-bonded interaction. Within the scatter graphs depicted in Fig. 8, the conspicuous spikes manifest distinct categorization

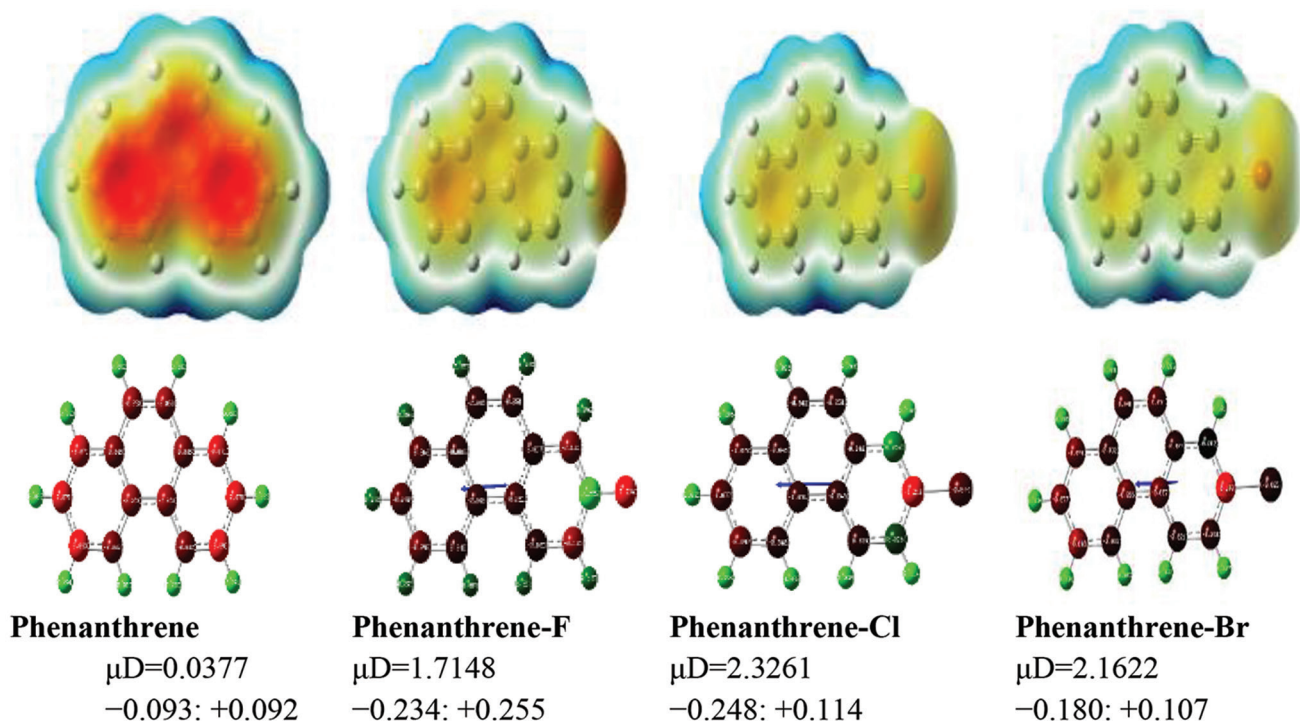| **Phenanthrene** | **Phenanthrene-F** | **Phenanthrene-Cl** | **Phenanthrene-Br** |
| μD=0.0377 | μD=1.7148 | μD=2.3261 | μD=2.1622 |
| −0.093: +0.092 | −0.234: +0.255 | −0.248: +0.114 | −0.180: +0.107 |

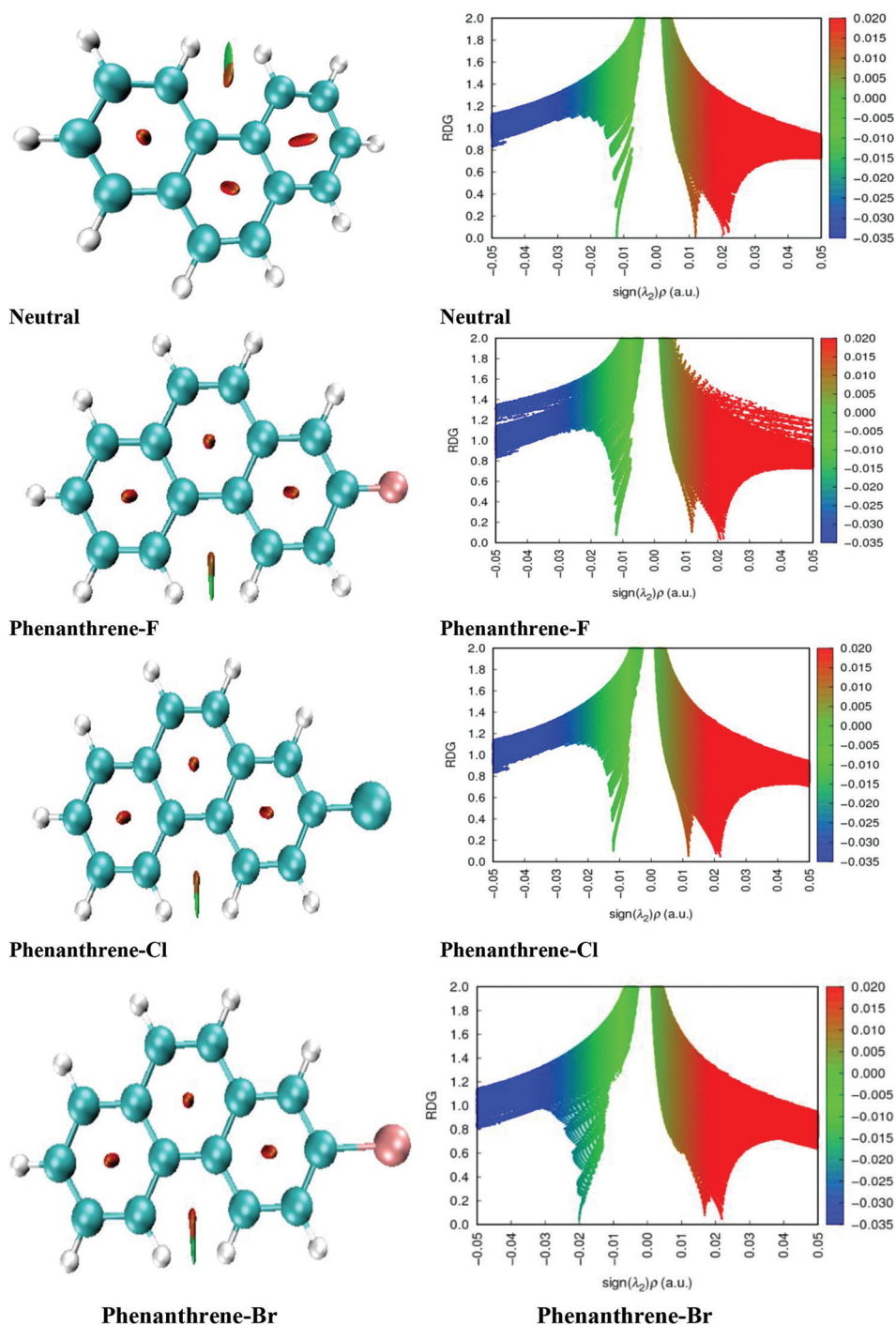Fig. 7. PEM and charge distributions for phenanthrene and its halogen-doped structures.

Fig. 8. RDG analysis of studied compounds – weak and strong interactions.

contingent upon the values of sign (λ2) ρ. These spikes correspond to three distinct regions, each characterized by its distinctive hue: red, green, and blue. The red region denotes intense repulsive interactions, attributed to steric hindrances. In contrast, the green region signifies feeble attractive forces akin to van der Waals interactions. Notably, the blue zone is emblematic of substantial intermolecular associations, particularly robust hydrogen bonding (Saidj, et al., 2023).

Compared to other compounds, it is noteworthy that compounds containing fluorine exhibit a notably higher density of points on the graph. This observation suggests that the weak hydrogen bonds and van Der Waals interactions within these fluorine-containing compounds possess enhanced strength. This is visually clear when examining Fig. 8, where regions colored in red are prominently concentrated within the aromatic rings. This observation serves to show a steric effect, indicative of substantial repulsive interactions within these regions. In the same Fig. 8, the appearance of a green-colored isosurface associated with the phenanthrene compound offers intriguing insights. This distinct green

isosurface shows van Der Waals (vdW) interactions. This isosurface's spatial arrangement within the phenanthrene compound points towards the existence of vdW interactions. In combination, these findings suggest a weak hydrogen bond interaction and supplementary contacts involving the two hydrogen atoms (H–H).

G. Drug Likeness

Assessing a compound's drug-likeness stands as a pivotal pursuit, frequently accomplished using Molinspiration property values, harmonizing with Lipinski's rule of five. This rule outlines that effective drugs generally meet designated thresholds: fewer than five hydrogen bond donors, less than ten hydrogen bond acceptors, molar refractivity between 40 and 160, polar surface area under 140 Å2, molecular weight below 500, and fewer than ten rotatable bonds (Walters and Murcko, 2002; Moore, et al., 2007; Arumugam, et al., 2013).

Table II showcases Molinspiration property values for diverse compounds, centered on phenanthrene and its halogen derivatives (+Cl, +Br, +F). These descriptors illuminate their hydrogen bonding potential, polarizability, and structural attributes. The compounds generally lack hydrogen bond donors, except for phenanthrene-fluorine, which exhibits hydrogen bond acceptor capability. Molar refractivity values subtly differ, implying variations in solubility and intermolecular interactions. Low polar surface area values align with expected low polarity and membrane permeability. Elevated molecular weights in halogenated compounds stem from halogen additions, and all compounds exhibit limited rotatable bonds, showing structural rigidity. These findings offer insights into these compounds' structural traits, interaction capacities, and potential applications.

H. Natural Bond Orbital (NBO) Analysis

The chemical under study underwent an in-depth exploration of its NBO configuration. The primary goal was to understand the interplay between its Lewis and non-Lewis orbitals, utilizing the B3LYP/6–31G(d, p) theoretical methodology. In addition, NBO analysis was executed using the same theoretical framework to uncover intramolecular and intermolecular hydrogen bonding and the dispersion of π electrons across the molecule. Stabilization energy, a measure of delocalization interactions, was determined using second-order energy for individual donor and acceptor NBOs, along with associated E(2) values depicting electron delocalization between donors and acceptors (Ranjith, et al., 2022; Sumathi, et al.; Abbaz, Bendjeddou and Villemin, 2017; Villemin, Abbaz and Bendjeddou, 2018; Abbaz, Bendjeddou and Villemin, 2018).

$$E^{(2)}q = \Delta E_{ij} = q_i \frac{F(i,j)^2}{\varepsilon_j - \varepsilon_i}$$

The symbol "qi" represents the occupancy of the donor orbital, while "εj" and "εi" denote diagonal elements, and "F(i,j)" signifies the diagonal NBO Fock matrix elements.

Table III presents a comprehensive Second Order Perturbation Theory Analysis of the Fock Matrix in NBO for Phenanthrene and its derivatives (+Cl, +Br, +F). The table elucidates the intricate interactions between donor and acceptor

Descriptors	Neutral	+Cl	+Br	+F	Expected range
Hydrogen bond donor (HBD)	0	0	0	0	<5
Hydrogen bond acceptors (HBA)	0	0	0	1	<10
Molar Refractivity	60.70	66.46	69.15	61.41	40–160
Polar surface area (PSA)	0	0	0	0	<140
Molecular weight	182.26	212.67	257.13	196.22	<500
Number of rotatable bonds	0	0	0	0	<10

TABLE III
SECOND-ORDER PERTURBATION THEORY ANALYSIS OF FOCK MATRIX IN NBO FOR STUDIED COMPOUNDS

Donor NBO (i)	Acceptor NBO (j)	E(2) kcal/mol	E(j)-E(i) a.u.	F(i,j) a.u.
Phenanthrene (neutral)				
π C1-C6	π* C2-C3	17.5	0.29	0.067
σ* C1-H7	σ C2-C3	4.48	1.07	0.062
π C2-C3	π* C1-C6	18.26	0.28	0.066
πC4-C5	π* C2-C3	17.64	0.29	0.067
π C11-C12	π* C2-C3	16.68	0.28	0.061
π C11-C12	π* C13-C14	14.49	0.28	0.061
π C11-C12	π*C17-C20	18.26	0.28	0.066
π C11-C12	π* C18-C19	17.85	0.28	0.065
π C17-C20	π*C11-C12	17.5	0.29	0.067
π C17-C20	π* C18-C19	18.4	0.29	0.066
Phenanthrene (+Cl)				
π C1-C6	π* C4-C5	18.27	0.29	0.066
π C2-C3	π* C1-C6	18.04	0.28	0.066
σ C3-C4	σ* C2-C3	4.16	1.23	0.064
π C4-C5	π* C1-C6	18.74	0.29	0.066
σ C4-H8	σ*C2-C3	4.94	1.06	0.065
π C11-C12	π* C17-C20	18.86	0.27	0.067
π C11-C12	π* C18-C19	19.83	0.26	0.066
σ C12-C19	σ*C18 -Cl24	5.58	0.82	0.061
LP (3) Cl 24	π*C18-C19	12.56	0.34	0.062
π*C18-C19	π* C11-C12	253.27	0.01	0.082
Phenanthrene (+Br)				
π C1-C6	π* C4-C5	19.4	0.28	0.066
σ C2-C3	σ* C2-C11	4.9	1.26	0.07
π C2-C3	π* C4-C5	18.13	0.27	0.066
π C2-C3	π* C11-C12	19.68	0.29	0.067
π C4-C5	π* C1-C6	19.82	0.28	0.067
π C4-C5	π* C2-C3	18.21	0.3	0.068
σ C11-C12	σ* C2-C11	4.97	1.27	0.071
σ C17-C20	σ*C18 -Br 24	5.26	0.79	0.058
LP (3) Br 24	π*C18-C19	10.27	0.31	0.054
π* C13-C14	π* C11-C12	230.06	0.01	0.08
Phenanthrene (+F)				
π C1-C6	π*C4-C5	18.21	0.29	0.065
π C2-C3	π* C1-C6	18.02	0.28	0.066
π C2-C3	π* C4-C5	17.89	0.28	0.066
π C4-C5	π* C1-C6	18.86	0.29	0.066
π C4-C5	π* C2-C3	17.62	0.29	0.067
σ C4-H8	σ * C2-C3	4.94	1.07	0.065
π C11-C12	π*C17-C20	19.95	0.27	0.068
π C11-C12	π*C18-C19	17.44	0.27	0.063
π C17-C20	π* C18-C19	20.83	0.29	0.07
LP (3) F24	π* C18-C19	19.24	0.43	0.087

NBOs, showcasing E(2) values that represent significant stabilization energies, differences in energy (E(j)-E(i)) in atomic

units, and F(i,j) values in atomic units. Notably, Phenanthrene (+Br) demonstrates a remarkable stabilization energy of 230.06 kcal/mol through the transition from π C11 - C12 to π* C13 - C14. The findings underscore that, while σ→σ* interactions generally possess lower delocalization energy, π→π* interactions dominate in this context. Resonance-induced interaction energies (n-π∗) contribute substantively to the overall molecular stability, providing valuable insights into the intricate nature of these interactions.

I. Non-linear Optical (NLO) Properties

NLO materials hold significance in non-linear optics, affecting IT and industries. Optimized geometry through B3LYP/6-31G+(d,p) was statically analyzed. Initial static hyper-polarizability (β_o), a 3D tensor, influences total dipole moment (μ_t), mean polarizability (α_o), and starting hyper-polarizability (Obot, et al., 2015, Ranjith, et al., 2022).

$$\mu_t = \left[\mu_x^2 + \mu_y^2 + \mu_z^2 \right]^{\frac{1}{2}}$$

$$\alpha_t = \left(\alpha_{xx} + \alpha_{yy} + \alpha_{zz} \right) / 3$$

$$\beta_t = \left(\beta_x^2 + \beta_y^2 + \beta_z^2 \right)^{1/2}$$

$$\beta_x = \beta_{xxx} + \beta_{xyz} + \beta_{xzz}$$

$$\beta_y = \beta_{yy} + \beta_{xxy} + \beta_{yzz}$$

$$\beta_z = \beta_{zzz} + \beta_{xxz} + \beta_{yzz}$$

The substantial magnitude of a specific component of polarizability and hyper-polarizability signifies a notable dispersion of charge in specific orientations (Khan, et al., 2021, Al-Shamiri, et al., 2022). The analysis of the NLO properties presented in Table IV provides insightful observations regarding various compounds (+Cl, +Br, +F) about the standard Urea benchmark. Notably, the dipole moment values for the investigated compounds consistently surpass that of Urea (μ = 1.3732 D), with the +Br derivative notably exhibiting a dipole moment of −2.16 D. In terms of polarizability, the results showcase phenanthrene's heightened responsiveness to a positive inductive effect (+F), demonstrating a polarizability value of −95.53 a.u., while phenanthrene displays the lowest polarizability under a positive inductive effect (+Br) at −87.00 a.u. However, the calculated hyper-polarizability (β_o) values for all compounds consistently fall short of the established Urea benchmark of 343.272×10⁻³³ esu. This collective finding suggests that the compounds may possess a limited potential for practical applications within NLO systems, causing further exploration. Importantly, the values provided in Table IV, initially reported in atomic units (a.u.), have been effectively converted to electrostatic units (e.s.u.) for improved clarity and comparison.

TABLE IV
NON-LINEAR OPTICAL PROPERTIES OF THE TITLE COMPOUNDS

Parameters	Phenanthrene			
	Phenanthrene			
	Neutral	+Cl	+Br	+F
μ_x	0.00	2.33	−2.16	−1.71
μ_y	0.00	−0.08	−0.08	−0.10
μ_z	−0.04	0.00	0.00	0.00
μ_t	0.04	2.33	2.16	1.71
α_{xx}	−87.94	−93.21	−94.36	−85.49
α_{yy}	−70.79	−81.24	−87.00	−73.47
α_{zz}	−71.07	−99.80	−105.25	−91.32
α_0	−76.60	−91.42	−95.53	−83.43
α (esu) × 10⁻²⁴	−11.35	−13.55	−14.16	−12.36
β_{xxx}	0.00	−60.39	68.17	−40.49
β_{xyy}	0.00	0.49	29.70	11.82
β_{xzz}	0.00	12.19	54.36	17.64
β_x	0.00	−47.70	152.23	−11.03
β_{yyy}	0.00	−1.05	2.56	−2.21
βxxy	0.00	0.20	0.58	−0.10
β_{yzz}	0.00	−0.28	−0.98	−0.67
β_y	0.00	−1.13	2.16	−2.98
β_{zzz}	−0.72	0.00	0.00	0.00
β_{xxz}	0.05	0.00	0.00	0.00
β_{yyz}	−0.55	0.00	0.00	0.00
β_z	−1.22	0.00	0.00	0.00
β_0 (esu) × 10⁻³³	1.22	47.72	152.24	11.43

IV. CONCLUSIONS

This comprehensive computational investigation provides an in-depth exploration of halogenated derivatives of phenanthrene, revealing their varied effects on molecular properties. Utilizing computational methods, the study examined electronic structure, reactivity, and complex behaviors. The interactions of halogens were highlighted through UV-Vis absorption spectra, NMR spectroscopy, PESs, and intermolecular interactions. In addition, the analysis of drug-likeness and NBO offered insights into the potential applications and intricate bonding patterns of these compounds. The investigation into NLO properties suggested practical applications as well. This journey culminated not only in theoretical insights but also in implications for fields such as medicine, environmental science, and organic electronics. The findings presented here enhance our understanding of halogenated phenanthrene derivatives and provide a foundation for further interdisciplinary research and applications.

REFERENCES

Abbaz, T., Bendjeddou, A., and Villemin, D., 2017. Structure, electronic properties, NBO, NLO and chemi-cal reactivity of bis (1, 4-dithiafulvalene) derivatives: Functional density theory study. *International Journal of Advanced Chemistry*, 6, pp.18-25.

Abbaz, T., Bendjeddou, A., and Villemin, D., 2018. Molecular structure, NBO analysis, first hyper polarizability, and homo-lumo studies of π-extended tetrathiafulvalene (EXTTF) derivatives connected to π-nitro phenyl by density functional method. *International Journal of Advanced Chemistry*, 6, p.114.

Abdel-Shafy, H.I., and Mansour, M.S.M., 2016. A review on polycyclic aromatic hydrocarbons: Source, environmental impact, effect on human health and remediation. *Egyptian Journal of Petroleum*, 25, pp.107-123.

Ahmed, L., and Rebaz, O., 2020. Computational study on paracetamol drug. *Journal of Physical Chemistry and Functional Materials,* 3, pp.9-13.

Aihara, J.I., 1999. Reduced HOMO-LUMO gap as an index of kinetic stability for polycyclic aromatic hydrocarbons. *The Journal of Physical Chemistry A,* 103, pp.7487-7495.

Akbas, E., Othman, K.A., Çelikezen, F.Ç., Aydogan Ejder, N., Turkez, H., Yapca, O.E., and Mardinoglu, A., 2023. Synthesis and biological evaluation of novel benzylidene thiazolo pyrimidin-3(5H)-one derivatives. *Polycyclic Aromatic Compounds*, 44, pp.1-18.

Al-Shamiri, H.A., Sakr, M.E., Abdel-Latif, S.A., Negm, N.A., Abou Kana, M.T., EL-Daly, S.A., and Elwahy, A.H., 2022. Experimental and theoretical studies of linear and non-linear optical properties of novel fused-triazine derivatives for advanced technological applications. *Scientific Reports,* 12, p.19937.

Arcadi, A., Fabrizi, G., Goggiamani, A., Iazzetti, A., Iavarone, F., Marrone, F., Mazzoccanti, G., and Sferrazza, A., 2023. Synthesis of 9,10-dibenzoyl-phenanthrene derivatives through a palladium-catalyzed domino approach. *Advanced Synthesis and Catalysis,* 365, pp.3277-3283.

Arfsten, D.P., Schaeffer, D.J., and Mulveny, D.C. 1996. The effects of near ultraviolet radiation on the toxic effects of polycyclic aromatic hydrocarbons in animals and plants: A review. *Ecotoxicology and Environmental Safety,* 33, pp.1-24.

Arumugam, M., Lulu, S., Kumari, S., and Veena, N., 2013. Computational screening and evaluation of bioactive compounds against NS3 helicase of HCV. *International Journal of Pharmacy and Pharmaceutical Sciences,* 5, pp.370-376.

Asath, R.M., Rekha, T., Premkumar, S., Mathavan, T., and Benial, A.M.F., 2016. Vibrational, spectroscopic, molecular docking and density functional theory studies on N-(5-aminopyridin-2-yl) acetamide. *Journal of Molecular Structure,* 1125, pp.633-642.

Aziz, S.B., Abdullah, O.G., Hussein, A.M., Abdulwahid, R.T., Rasheed, M.A., Ahmed, H.M., Abdalqadir, S.W., and Mohammed, A.R., 2017. Optical properties of pure and doped PVA: PEO based solid polymer blend electrolytes: Two methods for band gap study. *Journal of Materials Science: Materials in Electronics,* 28, pp.7473-7479.

Barbosa, F. Jr., Rocha, B.A., Souza, M.C.O., Bocato, M.Z., Azevedo, L.F., Adeyemi, J.A., Santana, A., and Campiglia, A.D., 2023. Polycyclic aromatic hydrocarbons (PAHs): Updated aspects of their determination, kinetics in the human body, and toxicity. *Journal of Toxicology and Environmental Health, Part B: Critical Reviews,* 26, pp.28-65.

Becke, A.D., 1993. Density-functional thermochemistry. III. The role of exact exchange. *The Journal of Chemical Physics,* 98, pp.5648-5652.

Boukabcha, N., Benmohammed, A., Belhachemi, M.H.M., Goudjil, M., Yahiaoui, S., Megrouss, Y., Djafri, A., Khelloul, N., Benyehlou, Z.D., and Djafri, A., 2023. Spectral investigation, TD-DFT study, Hirshfeld surface analysis, NCI-RDG, HOMO-LUMO, chemical reactivity and NLO properties of 1-(4-fluorobenzyl)-5-bromoindolin-2, 3dione. *Journal of Molecular Structure,* 1285, p.135492.

Ceylan, Ü., Tari, G.Ö., Gökce, H., and Ağar, E., 2016. Spectroscopic (FT–IR and UV-Vis) and theoretical (HF and DFT) investigation of 2-Ethyl-N-[(5-nitrothiophen-2-yl) methylidene] aniline. *Journal of Molecular Structure,* 1110, pp.1-10.

Chattaraj, P.K., and Roy, D.R., 2007. Update 1 of: electrophilicity index. *Chemical Reviews,* 107, pp.PR46-PR74.

Clar, E., 1972. Aromaticity of polyhedral boranes, carboranes, and metallacarboranes. *Angewandte Chemie International Edition in English,* 11, pp.1111-1115.

Costa, A.C. Jr., Ondar, G.F., Versiane, O., Ramos, J.M., Santos, T.G., Martin, A.A., Raniero, L., Bussi, G.G., and Tellez Soto, C.A., 2013. DFT: B3LYP/6-311G (d, p) vibrational analysis of bis-(diethyldithiocarbamate) zinc(II) and natural bond orbitals. *Spectrochimica Acta Part A: Molecular and Biomolecular Spectroscopy,* 105, pp.251-258.

Ding, Z.B., Tommasini, M., and Maestri, M., 2019. A topological model for predicting adsorption energies of polycyclic aromatic hydrocarbons on late-transition metal surfaces. *Reaction Chemistry and Engineering Journal,* 4, pp.410-417.

Domingo, L.R., Aurell, M.J., Pérez, P., and Contreras, R., 2002. Quantitative characterization of the global electrophilicity power of common diene/dienophile pairs in Diels–Alder reactions. *Tetrahedron,* 58, pp.4417-4423.

Esme, A., 2019. Experimental (FT-IR, FT-Raman, and UV–Vis) and quantum chemical calculations on monomer and dimer structures of l-hydroxy-2-naphthoic acid using the DFT and TD–DFT methods. *Indian Journal of Pure and Applied Physics,* 57, pp.822-835.

Haenen, H.T.M., 1977. Potential probe measurement analysis and charge distribution determination. *Journal of Electrostatics,* 2, pp.203-222.

Haritash, A.K., and Kaushik, C.P., 2009. Biodegradation aspects of polycyclic aromatic hydrocarbons (PAHs): A review. *Journal of Hazardous Materials,* 169, pp.1-15.

Humphrey, W., Dalke, A., and Schulten, K., 1996. VMD: Visual molecular dynamics. *Journal of Molecular Graphics,* 14, pp.33-38.

Jagdale, B.S., Ashok Adole, V., Bhavsing Pawar, T., and Desale, B.S., 2020. Molecular structure, frontier molecular orbitals, MESP and UV-visible spectroscopy studies of ethyl 4-(3,4-dimethoxyphenyl)-6-methyl-2-oxo-1,2,3,4-tetrahydropyrimidine-5-carboxylate: A theoretical and experimental appraisal. *Material Science Research India,* 17, pp.13-26.

Janietz, S., Bradley, D., Grell, M., Giebeler, C., Inbasekaran, M., and Woo, E., 1998. Electrochemical determination of the ionization potential and electron affinity of poly (9, 9-dioctylfluorene). *Applied Physics Letters,* 73, pp.2453-2455.

Kaka, K.N., Omer, R.A., Mamand, D.M., and Qader, A.F., 2024. Bromination of chalcone. *Aro-The Scientific Journal of Koya University,* 12, pp.48-53.

Khan, M.U., Khalid, M., Asim, S., Momina, Hussain, R., Mahmood, K., Iqbal, J., Akhtar, M.N., Hussain, A., and Imran, M., 2021. Exploration of nonlinear optical properties of triphenylamine-dicyanovinylene coexisting donor-π-acceptor architecture by the modification of π-conjugated linker. *Frontiers in Materials,* 8, p.719971.

Koparir, P., Omar, R.A., Sarac, K., Ahmed, L.O., Karatepe, A., Taskin-Tok, T., and Safin, D.A., 2023. Synthesis, characterization and computational analysis of thiophene-2, 5-diylbis ((3-mesityl-3-methylcyclobutyl) methanone). *Polycyclic Aromatic Compounds,* 43, pp.6107-6125.

Koparir, P., Parlak, A.E., Karatepe, A., and Omar, R.A., 2022. Elucidation of potential anticancer, antioxidant and antimicrobial properties of some new triazole compounds bearing pyridine-4-yl moiety and cyclobutane ring. *Arabian Journal of Chemistry,* 15, p.103957.

Lawal, A.T., and Fantke, P., 2017. Polycyclic aromatic hydrocarbons. A review. *Cogent Environmental Science,* 3, p.1339841.

Lazarou, Y.G., Prosmitis, A.V., Papadimitriou, V.C., and Papagiannakopoulos, P., 2001. Theoretical calculation of bond dissociation energies and enthalpies of formation for halogenated molecules. *The Journal of Physical Chemistry A,* 105, pp.6729-6742.

Li, A., and Draine, B., 2002. Do the infrared emission features need ultraviolet excitation? The polycyclic aromatic hydrocarbon model in UV-poor reflection nebulae. *The Astrophysical Journal,* 572, p.232.

Li, S., Zhang, Q., Gao, M., Li, H., Yang, Z., Wang, Y., and Sun, H., 2024. Polycyclic aromatic hydrocarbons and their halogenated derivatives in soil from Yellow River Delta: Distribution, source apportionment, and risk assessment. *Marine Pollution Bulletin,* 202, p.116308.

Li, W., and Wu, S., 2023. Challenges of halogenated polycyclic aromatic hydrocarbons in foods: Occurrence, risk, and formation. *Trends in Food Science and Technology,* 131, pp.1-13.

Li, Z., Hu, W., Li, Z., and Wang, Z., 2020. High performance n-type organic field-effect transistors based on halogenated derivatives of naphthalene tetracarboxylic

diimides. *Materials Science in Semiconductor Processing,* 120, p.105273.

Lu, T., and Chen, F., 2012. Multiwfn: A multifunctional wavefunction analyzer. *Journal of Computational Chemistry,* 33, pp.580-592.

Makula, P., Pacia, M., and Macyk, W., 2018. How to correctly determine the band gap energy of modified semiconductor photocatalysts based on UV-Vis spectra. *The Journal of Physical Chemistry Letters,* 9, pp.6814-6817.

Mayr, H., and Patz, M., 1994. Scales of nucleophilicity and electrophilicity: A system for ordering polar organic and organometallic reactions. *Angewandte Chemie International Edition in English,* 33, pp.938-957.

McClellan, A.L., and Pimentel, G.C., 1955. Vibrational assignment and thermodynamic properties of naphthalene. *The Journal of Chemical Physics,* 23, pp.245-248.

McCoull, K.D., Rindgen, D., Blair, I.A., and Penning, T.M., 1999. Synthesis and characterization of polycyclic aromatic hydrocarbon o-quinone depurinating N7-guanine adducts. *Chemical Research in Toxicology Journal,* 12, pp.237-46.

Modelli, A., Mussoni, L., and Fabbri, D., 2006. Electron affinities of polycyclic aromatic hydrocarbons by means of B3LYP/6-31+G* calculations. *The Journal of Physical Chemistry A,* 110, pp.6482-6486.

Montgomery, J.A., Frisch, M.J., Ochterski, J.W., and Petersson, G.A., 1999. A complete basis set model chemistry. VI. Use of density functional geometries and frequencies. *The Journal of Chemical Physics,* 110, pp.2822-2827.

Moore, T.J., Cohen, M.R.A., and Furberg, C.D., 2007. A decade of drug-likeness. *Nature Reviews Drug Discovery,* 6, pp.853-853.

Nasidi, I.I, Kaygili, O., Majid, A., Bulut, N., Alkhedher, M., and Eldin, S.M., 2022. Halogen doping to control the band gap of ascorbic acid: A theoretical study. *ACS Omega,* 7, pp.44390-44397.

Obot, I., Macdonald, D., and Gasem, Z., 2015. Density functional theory (DFT) as a powerful tool for designing new organic corrosion inhibitors. Part 1: An overview. *Corrosion Science,* 99, pp.1-30.

Omar, R.A., Koparir, P., Sarac, K., Koparir, M., and Safin, D.A., 2023. A novel coumarin-triazole-thiophene hybrid: Synthesis, characterization, ADMET prediction, molecular docking and molecular dynamics studies with a series of SARS-CoV-2 proteins. *Journal of Chemical Sciences,* 135, p.6.

Omer, R., Koparir, P., Koparir, M., Rashid, R., Ahmed, L., and Hama, J., 2022a. Synthesis, characterization and DFT study of 1-(3-Mesityl-3-methylcyclobutyl)-2-((4-phenyl-5-(thiophen-2-yl)-4H-1, 2, 4-triazol-3-yl) thio) ethan-1-one. *Protection of Metals and Physical Chemistry of Surfaces,* 58, pp.1077-1089.

Omer, R.A., Ahmed, K.M., Othman, K.A., Hamad, W.M., Faraj, R.K., Muhialdin, A.J., and Salih, S.K., 2024. New thiazole derivatives. *Aro-The Scientific Journal of Koya University,* 12, pp.10-22.

Omer, R.A., Koparir, P., and Ahmed, L., 2022b. Theoretical determination of corrosion inhibitor activities of 4-allyl-5-(pyridin-4-yl)-4H-1, 2, 4-triazole-3-thiol-thione tautomerism. *Indian Journal of Chemical Technology,* 29, pp.75-81.

Palmer, A.J., Ghani, R.A., Kaur, N., Phanstiel, O., and Wallace, H.M., 2009. A putrescine-anthracene conjugate: A paradigm for selective drug delivery. *Biochemical Journal,* 424, pp.431-438.

Pearson, R.G., 2005. Chemical hardness and density functional theory. *Journal of Chemical Sciences,* 117, pp.369-377.

Pi, X., Sun, F., Gao, J., Qu, Z., Wang, A., Qie, Z., Wang, L., and Liu, H., 2019. A new insight into the SO(2) adsorption behavior of oxidized carbon materials using model adsorbents and DFT calculations. *Physical Chemistry Chemical Physics,* 21, pp.9181-9188.

Ranjith, P., Ignatious, A., Panicker, C.Y., Sureshkumar, B., Armakovic, S., Armakovic, S.J., Van Alsenoy, C., and Anto, P., 2022. Spectroscopic investigations, DFT calculations, molecular docking and MD simulations of 3-[(4-Carboxyphenyl) carbamoyl]-4-hydroxy-2-oxo-1, 2-dihydroxy quinoline-6-carboxylic acid. *Journal of Molecular Structure,* 1264, p.133315.

Rebaz, O., Ahmed, L., Koparir, P., and Jwameer, H., 2022. Impact of solvent polarity on the molecular properties of dimetridazole. *El-Cezeri,* 9**,** pp.740-747.

Ricks, A.M., Douberly, G.E., and Duncan, M.A., 2009. The infrared spectrum of protonated naphthalene and its relevance for the unidentified infrared bands. *The Astrophysical Journal,* 702**,** p.301.

Roy, C.P., Karmakar, S., and Dash, J., 2024. Synthesis of phenanthrenes and 1-hydroxyphenanthrenes via aromatization-assisted ring-closing metathesis: Toward polynuclear aromatic hydrocarbons. *The Journal of Organic Chemistry,* 89, pp.10511-10523.

Ryno, S., 2015. Molecular-Scale Understanding of Electronic Polarization in Organic Molecular Crystals. *Georgia Institute of Technology,* p.1-12.

Sahoo, B.M., Ravi Kumar, B.V.V., Banik, B.K., and Borah, P., 2020. Polyaromatic hydrocarbons (PAHs): Structures, synthesis and their biological profile. *Current Organic Synthesis,* 17, pp.625-640.

Saidj, M., Djafri, A., Rahmani, R., Belkafouf, N.E.H., Boukabcha, N., Djafri, A., and Chouaih, A., 2023. Molecular structure, experimental and theoretical vibrational spectroscopy,(HOMO-LUMO, NBO) investigation,(RDG, AIM) analysis,(MEP, NLO) study and molecular docking of Ethyl-2-{[4-Ethyl-5-(Quinolin-8-yloxyMethyl)-4H-1, 2, 4-Triazol-3-yl] Sulfanyl} acetate. *Polycyclic Aromatic Compounds,* 43, pp.2152-2176.

Sarmah, A., and Hobza, P., 2020. Directly linked metalloporphyrins: A quest for bio-inspired materials. *Materials Advances,* 1, pp.1895-1908.

Solano, E.A., and Mayer, P.M., 2015. A complete map of the ion chemistry of the naphthalene radical cation? DFT and RRKM modeling of a complex potential energy surface. *The Journal of Chemical Physics,* 143, 104305.

Srivastava, A., and Singh, V.B., 2007. Theoretical and experimental studies of vibrational spectra of naphthalene and its cation. *Indian Journal of Pure and Applied Physics,* 45, pp.714-720.

Sumathi, D., Thanikachalam, V., Bharanidharan, S., Saleem, H., and Babu, N.R. Vibrational spectroscopy (FT-IR, FT-Raman and UV) studies of E-[1-Methyl-2, 6-diphenyl-3-(propan-2-yl) piperidin-4-ylidene] amino 3-methylbenzoate] using DFT method. *International Journal of Scientific Research,* 5, pp. 2277-8179.

Sun, Z., and Wu, J., 2012. Open-shell polycyclic aromatic hydrocarbons. *Journal of Materials Chemistry,* 22, pp.4151-4160.

Swofford, R.L., Long, M.E., and Albrecht, A.C., 1976. C-H vibrational states of benzene, naphthalene, and anthracene in the visible region by thermal lensing spectroscopy and the local mode model. *The Journal of Chemical Physics,* 65, pp.179-190.

Tang, M., Yu, Q., Wang, Z., Zhang, C., Sun, B., Yi, Y., and Zhang, F.L., 2018. Synthesis of polycyclic aromatic hydrocarbons (PAHs) via a transient directing group. *Organic Letters,* 20, pp.7620-7623.

Tang, M.L., and Bao, Z., 2011. Halogenated materials as organic semiconductors. *Chemistry of Materials,* 23, pp.446-455.

Tirado-Rives, J., and Jorgensen, W.L., 2008. Performance of B3LYP density functional methods for a large set of organic molecules. *Journal of Chemical Theory and Computation,* 4, pp.297-306.

Toriyama, M.Y., Ganose, A.M., Dylla, M., Anand, S., Park, J., Brod, M.K., Munro, J.M., Persson, K.A., Jain, A., and Snyder, G.J., 2022. How to analyse a density of states. *Materials Today Electronics,* 1, p.100002.

Villemin, D., Abbaz, T., and Bendjeddou, A., 2018. Molecular structure, HOMO, LUMO, MEP, natural bond orbital analysis of benzo and anthraquinodimethane derivatives. *Pharmaceutical and Biological Evaluations,* 5, p.27.

Walters, W.P., and Murcko, M.A., 2002. Prediction of "drug-likeness". *Advanced Drug Delivery Reviews,* 54, pp.255-271.

Wang, D., Chen, L., Shi, C., Wang, X., Cui, G., Zhang, P., and Chen, Y., 2016. Quantum spin Hall insulator in halogenated arsenene films with sizable energy

gaps. *Scientific reports,* 6, p.28487.

Wilbur, D., Manning, W.B., Hilton, B.D., and Muschik, G.M., 1982. Carbon-13 NMR of polycyclic aromatic compounds. 1-Methoxybenz[a]anthracene-7, 12-diones. *Organic Magnetic Resonance,* 18, pp.63-67.

Wodrich, M.D., Corminboeuf, C., Schreiner, P.R., Fokin, A.A., and Schleyer, P.V.R., 2007. How accurate are DFT treatments of organic energies? *Organic Letters,* 9, pp.1851-1854.

Wu, M., Nie, M., Wang, X., Su, J., and Cao, W., 2010. Analysis of phenanthrene biodegradation by using FTIR, UV and GC-MS. *Spectrochimica Acta Part A: Molecular and Biomolecular Spectroscopy,* 75, pp.1047-1050.